A Comparison of Contemporaneous Airborne Altimetry and Ice-Thickness Measurements of Antarctic Ice Shelves

Complete List of Authors:
Chartrand, Allison; (allisonchartrand@gmail.com)
The Ohio State University Byrd Polar and Climate
Research Center, School of Earth Sciences

Howat, Ian; (ihowat@gmail.com)
The Ohio State University Byrd Polar and Climate Research
Center, School of Earth Sciences

This is a non-peer reviewed preprint submitted to EarthArXiv. This paper was submitted for peer review in the Journal of Glaciology.

Author Twitter handle: @IceShelvesAndAC

JOURNAL OF GLACIOLOGY

CAMBRIDGE UNIVERSITY PRESS

THIS MANUSCRIPT HAS BEEN SUBMITTED TO THE JOURNAL OF GLACIOLOGY AND HAS NOT BEEN PEER-REVIEWED.

A Comparison of Contemporaneous Airborne Altimetry and Ice-Thickness Measurements of Antarctic Ice Shelves

Journal:	*Journal of Glaciology*
Manuscript ID	Draft
Manuscript Type:	Article
Date Submitted by the Author:	n/a
Complete List of Authors:	Chartrand, Allison; The Ohio State University Byrd Polar and Climate Research Center, School of Earth Sciences Howat, Ian; The Ohio State University Byrd Polar and Climate Research Center, School of Earth Sciences
Keywords:	Ice shelves, Ice thickness measurements, Remote sensing, Radio-echo sounding, Antarctic glaciology
Abstract:	Estimates of ice shelf mass loss are dependent on the assumption of hydrostatic equilibrium to estimate ice thickness from surface height measurements, especially when ice and firn thickness measurements are unavailable. Recent investigations have challenged the assumption that ice shelves are freely floating, particularly in proximity to structures such as basal channels and shear margins. We compare contemporaneous ice penetrating radar thickness measurements and laser altimetry-derived hydrostatic thickness estimates from multiple airborne surveys on Antarctic ice shelves. On average, the hydrostatic assumption overestimates ice shelf thickness by ~13 m +/- 45 m, but this difference

	varies widely within and among the ice shelves surveyed. We find that small changes in firn thickness can account for the imbalance in most locations, but that uncertainties in firn thickness or density cannot explain all discrepancies. Errors in ice shelf thickness estimated using the hydrostatic assumption did not, on average, significantly change the estimated basal melt rate at a given point (<2% difference). Our results indicate that localized approaches to estimating ice shelf thickness and rates of change are not applicable at large scales, and vice versa.

SCHOLARONE™
Manuscripts

A Comparison of Contemporaneous Airborne Altimetry and Ice-Thickness Measurements of Antarctic Ice Shelves

A.M. Chartrand, I.M. Howat

Byrd Polar and Climate Research Center, The Ohio State University, Columbus, OH, USA

Correspondence: Allison Chartrand <allisonchartrand@gmail.com>

ABSTRACT. Estimates of ice shelf mass loss are dependent on the assumption of hydrostatic equilibrium to estimate ice thickness from surface height measurements, especially when ice and firn thickness measurements are unavailable. Recent investigations have challenged the assumption that ice shelves are freely floating, particularly in proximity to structures such as basal channels and shear margins. We compare contemporaneous ice penetrating radar thickness measurements and laser altimetry-derived hydrostatic thickness estimates from multiple airborne surveys on Antarctic ice shelves. On average, the hydrostatic assumption overestimates ice shelf thickness by ~13 m +/- 45 m, but this difference varies widely within and among the ice shelves surveyed. We find that small changes in firn thickness can account for the imbalance in most locations, but that uncertainties in firn thickness or density cannot explain all discrepancies. Errors in ice shelf thickness estimated using the hydrostatic assumption did not, on average, significantly change the estimated basal melt rate at a given point (<2% difference). Our results indicate that localized approaches to estimating ice shelf thickness and rates of change are not applicable at large scales, and vice versa.

1. INTRODUCTION

Estimates of ice shelf mass loss are strongly dependent on the assumption of hydrostatic equilibrium, especially when ice thickness measurements are unavailable. The assumption that the ice shelf is freely floating allows estimates of ice thickness from surface height measurements alone. Recent investigations, however, provide evidence that some areas of ice shelves are not freely floating, particularly in regions associated with steep gradients in ice thickness, such as basal channels and shear margins (e.g., Drews, 2015; Drews and others, 2016; Le Brocq and others, 2013; Dow and others, 2021; Chartrand and Howat 2020; Alley and others, 2019). However, the spatial scales of this imbalance and their impacts on ice shelf thickness and mass balance estimates are unknown.

The validity of the hydrostatic assumption has been investigated several times, though rarely with contemporaneous surface height and ice thickness data. The hydrostatic assumption was used to compare ice surface heights from the European Remote Sensing Satellite, ERS-1 (launched in 1991), to surface heights derived from Ross Ice Shelf Geophysical and Glaciological Survey (RIGGS) and Scott Polar Research Institute ice penetrating radar (IPR) surveys from the 1970s (Bamber and Bentley, 1994). They found agreement between the two datasets within the combined errors of the measurements across the Ross Ice Shelf, with some exceptions near grounding lines and in the vicinity of flow stripes. Later, ERS-1 data from 1994-1995 were supplemented by ICESat laser altimetry to derive a 1-km resolution gridded ice thickness dataset for all Antarctic ice shelves, and these results were compared to several independent airborne RES-derived thickness datasets, with varying levels of agreement depending on proximity to the grounding line, data gaps, and unknown marine ice density and thickness (Griggs and Bamber, 2011). Chuter and Bamber (2015) compared 1 km-resolution gridded ice thickness estimates derived from Cryosat-2 radar altimetry from 2011-2014 to IPR thickness measurements from 2001 and earlier on the Amery Ice Shelf, showing a mean difference in thickness of ~3% between the two estimates.

Observed and estimated ice shelf thickness from contemporaneous, or nearly contemporaneous, IPR and surface elevation measurements have been compared on smaller spatial scales, particularly in investigations of basal channels (e.g., Chartrand and Howat, 2020; Dow and others, 2021), showing that the hydrostatic assumption underestimates variability in ice thickness over distances <1 km. Similarly, simulations of stress fields on ice shelves have shown that the ice surface above basal channels is maintained at a higher elevation than expected based on ice thickness and the hydrostatic assumption, likely due to bridging stresses (Drews, 2015; Le Brocq and others, 2013).

Accurate measurements and/or estimates of ice shelf thickness are crucial for mass balance estimates and discharge of ice across the grounding line. Disagreement between observed and hydrostatic thickness has consistently been identified near grounding lines, where ice is generally thinner than expected under the hydrostatic assumption, perhaps due to high densities of ice draining fast-flowing glaciers and ice streams, and/or tidal flexure in the grounding zone (Bamber and Bentley, 1994; Bindschadler and others, 2011; Griggs and Bamber, 2011; Chuter and Bamber, 2015), leading to uncertainties in ice flux and mass balance estimates, and sub-ice shelf and ice sheet models. Furthermore, disagreements between observed and hydrostatic thickness on sub-kilometer scales and near ice fronts (e.g., in regions of accreted marine ice), introduce inaccuracies in estimates of basal mass change and the impact of small-scale features like basal channels on ice shelf stability (Bamber and Bentley 1994; Griggs and Bamber, 2011; Chuter and Bamber, 2015; Drews, 2015).

Over a decade of ice shelf thickness measurements from airborne ice penetrating radar (IPR) collected by the NASA Operation IceBridge (OIB) and pre-OIB and NSF Investigating the Cryospheric Evolution of the Central Antarctic Plate (ICECAP) projects provide an extensive dataset with which to examine possible deviations from hydrostatic equilibrium on Antarctic ice shelves (MacGregor and others, 2021). Here, we use IceBridge Multichannel Coherent Radar Depth Sounder (MCoRDS) and ICECAP High Capability Radar Sounder (HiCARS) IPR measurements and Airborne Topographic Mapper (ATM) and Riegl laser altimetry to compare measured thickness and hydrostatic thickness on sub-kilometer and ice-shelf scales, and elucidate the implications of the hydrostatic assumption.

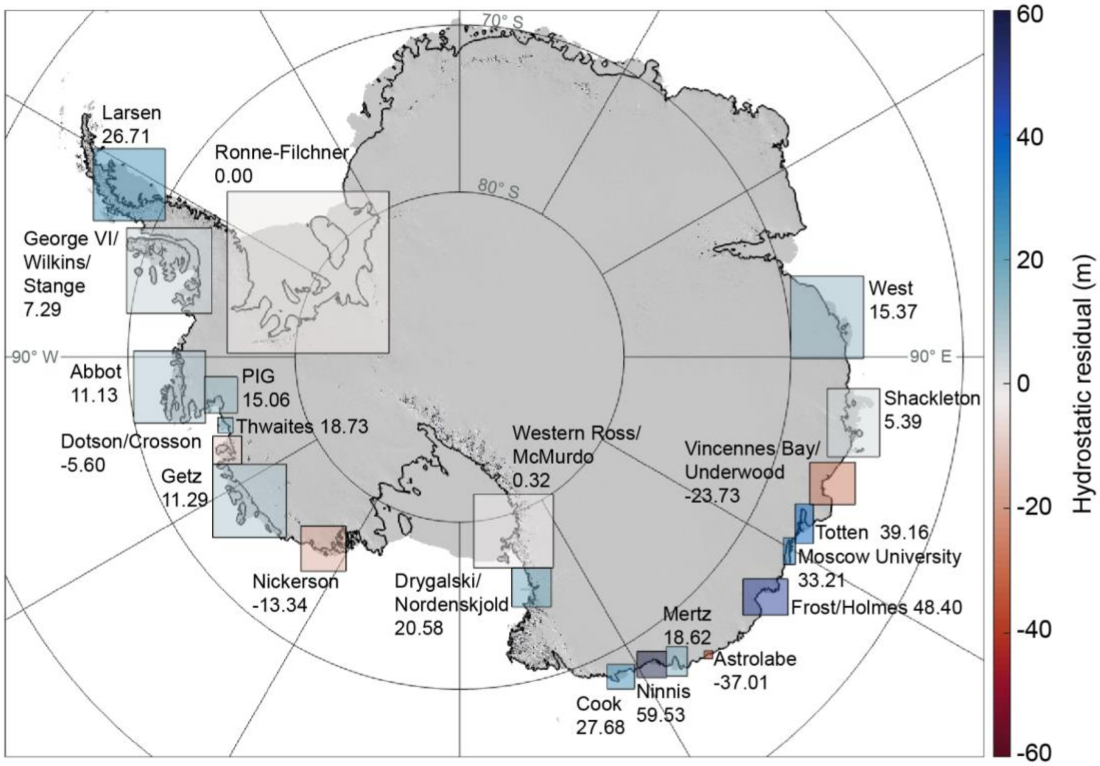

Figure 1. Map of Antarctica showing the ice shelf system boundaries (boxes) colored by the mean hydrostatic residual. Base map is the REMA DEM hillshade image, and the black curve shows the 2007-2009 InSAR grounding line.

2. DATASETS

Ice thickness measurements, H, are obtained from the MCoRDS L2 datasets from both pre-OIB campaigns and OIB campaigns. (Paden and others, 2011; Paden and others, 2010) These data have coverage over most of the West Antarctic coast, and limited coverage on the larger Ronne and Filchner ice shelves and their tributary glaciers.

Ice thickness measurements are also obtained from the HiCARS 1 and 2 L2 datasets from OIB and the ICECAP project (Blankenship and others, 2011; Blankenship and others, 2012a). These data have coverage over much of the East Antarctic coast between the Ross Ice Shelf and West Ice Shelf.

Surface elevation data, z, collected contemporaneously with MCoRDS thickness data were obtained from the pre-OIB and OIB Airborne Topographic Mapper (ATM) L1B datasets at NSIDC (Studinger, 2012; Studinger, 2013). Surface elevation data collected contemporaneously with HiCARS thickness data were obtained from the OIB/ICECAP Riegl Laser Altimeter L2 dataset at NSIDC (Blankenship and others, 2012b).

Gridded firn air column thickness values, H_a, were obtained from the steady-state firn model (Ligtenberg and others, 2011) reported in BedMachine Antarctica at NSIDC (Morlighem, and others 2020), and bilinearly interpolated to the MCoRDS/HiCARS ground track coordinates. H_a is defined as the length of the change in firn thickness resulting from compressing the firn column to ice density (Ligtenberg and others, 2011).

Only OIB and ICECAP campaigns in which MCoRDS/HiCARS thickness and ATM/Riegl surface elevation data were collected simultaneously are used in this study. To ensure the highest quality comparison between datasets, the data are first filtered by removing all data with quality flags. Contemporaneous ATM and Riegl surface elevation data *z* are then interpolated to MCoRDS/HiCARS ground track coordinates using natural neighbor triangulation with no extrapolation. All *z* data are corrected and referenced to heights relative to mean sea level, or freeboard heights *h* by correcting for the geoid height and mean dynamic topography (MDT) such that *h = z - tide - geoid - MDT*. The Eigen-6C4 geoid included in BedMachine Antarctica is used (Förste and others, 2014; Morlighem and others, 2020), and MDT values are obtained from the DTU10 model (Andersen and Knudsen, 2009); these gridded data are bilinearly interpolated to the ground track coordinates. Tide corrections are obtained from the CATS2008b tide model (Padman and others, 2018). All data upstream of the MEaSUREs Antarctic Grounding Line from Differential Satellite Radar Interferometry from the 2007-2009 IPY are removed (Mouginot and others, 2017; Rignot and others, 2013).

Contemporaneous surface and thickness data are binned by discrete ice shelves or ice shelf systems (Fig. 1). Thus, MCoRDS data are binned for nine ice shelf systems in West Antarctica and the Antarctic Peninsula, including the Ronne-Filchner Ice Shelf, and HiCARS data are binned into an additional twelve discrete ice shelf systems, including the Western Ross/McMurdo Ice Shelf and several others in East Antarctica (Fig. 1). The surface height data are further quality-controlled by comparison with the Reference Elevation Model of Antarctica (REMA) 200 m Digital Elevation Model (DEM) mosaic (Howat and others, 2019; Howat and others, 2022). REMA surface heights are bilinearly interpolated to the ground track coordinates for each ice shelf, and ATM/Riegl surface heights that differ from REMA by more than 2.5 times the mean absolute deviation of surface height for each ice shelf are removed. This window is used to avoid exclusion of airborne observations that differ from REMA due to advection of surface features, but to exclude erroneous observations due to clouds or measurement errors. All surface height and thickness data less than 20 m in magnitude are removed, as these data likely reflect open ocean or sea ice, and all ground track points where firn air content, H_a, exceeded surface height are removed, as these are likely erroneous.

3. ESTIMATING HYDROSTATIC RESIDUAL AND ERRORS

The hydrostatic ice shelf thickness, H_E, is calculated at each MCoRDS and HiCARS ground track coordinate from the contemporaneous altimeter-measured freeboard height, *h*, as

$$H_E = h\frac{\rho_s}{\rho_s-\rho_i} - H_a\frac{\rho_a-\rho_i}{\rho_i-\rho_s}, \quad (1)$$

where ρ_s is seawater density (1,027 kg m^{-3}), ρ_i is meteoric ice density (918 kg m^{-3}), ρ_a is the firn-air column density (2 kg m^{-3}), and H_a is the thickness of the firn-air column within the freeboard, and the subscript *E* denotes that H_E is an estimate of the hydrostatic thickness of the full ice column (Fig. 2). The difference between the estimated hydrostatic thickness H_E and the observed thickness *H* is defined as the hydrostatic residual, or *R*:

$$R = H_E - H. \quad (2)$$

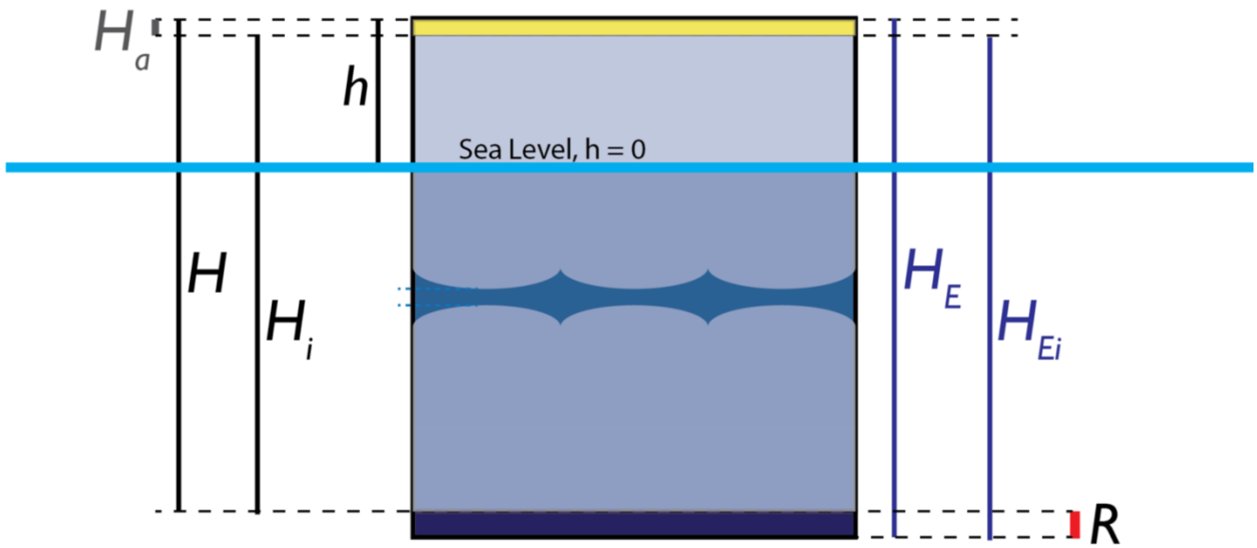

Figure 2. Schematic showing relevant quantities for a column of ice floating in seawater. The ice below sea level is discontinuous to exaggerate the vertical scale. Quantities on the left of the ice column represent observed values for an ice column that is not necessarily in hydrostatic equilibrium. H: total observed ice thickness; h: observed freeboard thickness / surface height; H_a: thickness of the firn air column; $H_i = H - H_a$; Quantities on the right represent values for an ice column with the observed freeboard height, h, in hydrostatic equilibrium, calculated using Eqn (1). H_E: total hydrostatic ice thickness; $H_{Ei} = H_E - H_a$; R is equal to the difference between H_E and H.

Thus, a positive value for R indicates that the actual ice thickness is less than hydrostatic thickness, or that the ice surface is elevated relative to sea level (Fig. 2), with the opposite for a negative R. We expect R to depend on measurement errors, assumptions in ice density and firn thickness, and ice dynamics, such as transfer of vertical stresses.

3.1. Uncertainties and Errors

Uncertainties in MCoRDS ice thicknesses are estimated to be ± 50 m (Medley and others, 2014), and HiCARS ice thicknesses have a reported uncertainty of ± 70 m (Blankenship and others, 2011). However, since these are nominal values with potentially different values over ice shelves, we perform a crossover analysis to assess the self-consistency of the data. Crossover points are located by splitting the ground tracks into 5000-point segments for each ice shelf over which data were collected, and by finding all intersections of all possible combinations of 5000-point segments. This method identifies intersections not only where the ground tracks cross one another at large angles, but also where repeated ground tracks overlap. Where repeated ground tracks overlap, the intersections are frequently only meters apart. We thus use a visual inspection to select repeat-track intersections that are at least 1 km apart and ignore the rest to ensure that redundant points aren't included in our analyses. All measurements that fall within 50 m of an intersection point are differenced from each other, showing expected changes in thickness through time. Including only same-campaign observations, crossover or repeat-track intersections within the MCoRDS dataset have a mean absolute difference in H of 3.3 m and a standard deviation of H of ± 2.6 m. For HiCARS, the mean absolute difference in H at same-campaign intersections is 3.6 m and the standard deviation in H is ± 4.1 m. Thus, we adopt a conservative error of ± 5 m in the MCoRDS and HiCARS thickness data. We do not consider errors or uncertainties in $\boldsymbol{\rho}_s$, which varies by < 1 kg m^{-3} in the top 1 km of the ocean (Jackett and McDougall, 1997), or $\boldsymbol{\rho}_i$, which has accepted values ranging from 910-921 kg m^{-3} and often varies by less than ± 5 kg m^{-3} (e.g., Griggs and Bamber, 2011), choosing to keep these values constant throughout our analyses. Errors for other data sets and calculations are reported in Table 1.

Propagating the above errors and uncertainties in Eqns (1) and (2) gives a combined error of ± 44.7 m for H_E and ± 45.0 m for R. It's unclear, however, how much this error varies spatially due to its dependence on the firn correction.

Table 1. Errors/Uncertainties for data involved in the calculation of *R*.

Dataset	**Reported Error (±)**	**Reference**
MCORDS Thickness	50 m (reduced to 5 m in crossover analysis)	Medley and others, 2014
HiCARS Thickness	70 m (reduced to 5 m in crossover analysis)	Blankenship and others, 2011
LiDAR surface height	0.1 m	Martin and others, 2012; Blankenship and others, 2013
Tide correction	0.1 m	Padman and others, 2002
Mean Dynamic Topography (MDT)	0.1 m	Andersen and others, 2018
Geoid height	0.3 m	Förste and others, 2014
Firn correction	10 m	Ligtenberg and others, 2014
Propagated Error for H_E	44.7 m	
Propagated Error for R	45.0 m	

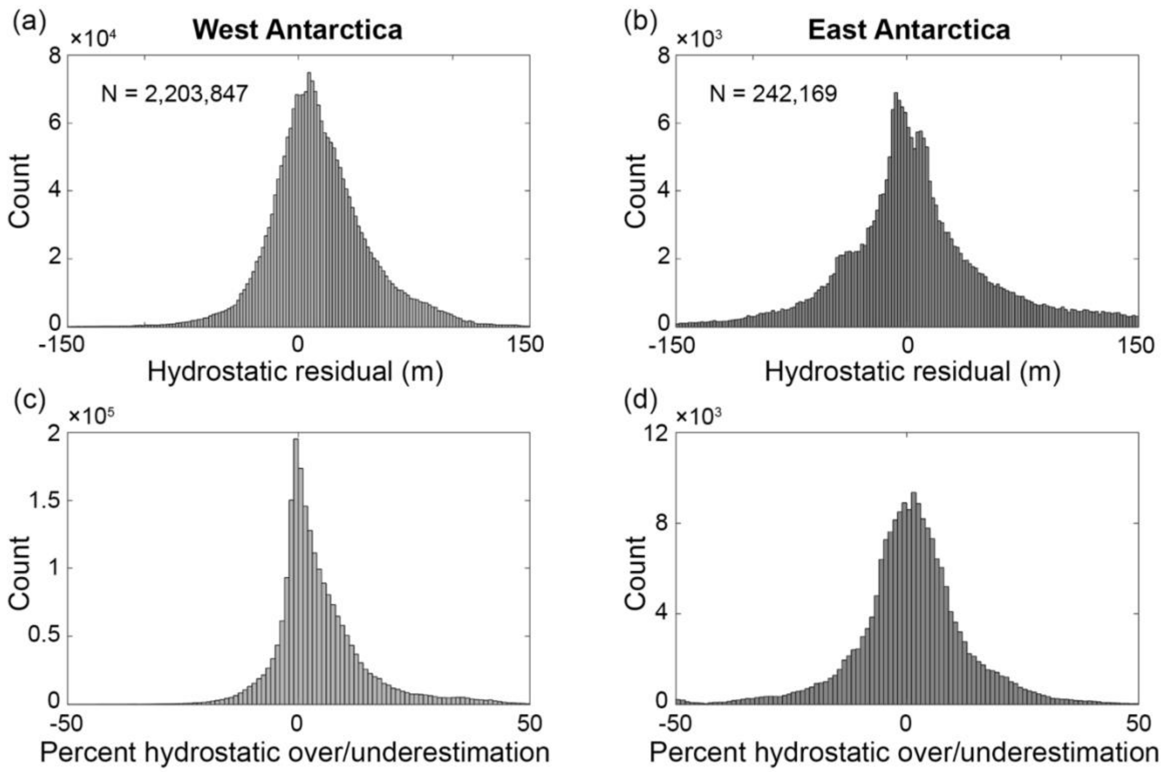

Figure 3. Histograms of (a, b) *R* and (c, d) percent difference between hydrostatic and measured ice thickness for all MCoRDS (West Antarctica, a, c) and HiCARS (East Antarctica, b, d) data used in analysis.

4. RESULTS

4.1. Hydrostatic Residual

Analyses of the hydrostatic residual, *R*, are performed for individual ground tracks, sectors of ice shelf regions, whole ice shelves, and for the complete dataset. To remove outliers, data are binned by 100 m intervals of *H* at the corresponding ground track coordinates. We then remove measurements where $R <$ Q1 - 1.5*IQR or $R >$ Q3 + 1.5*IQR, where Q1 and Q3 are the 25% and 75% percentiles of the binned *R* values, respectively, and IQR = Q3 - Q1 is the interquartile range.

For the nine West Antarctic ice shelf systems with contemporaneous ATM and MCoRDS measurements, the mean *R* is ~7.9 m (2.1% of measured ice thickness). In other words, the observed ice thickness is 7.9 m less, on average, than the hydrostatic thickness estimated from surface height. The hydrostatic residual varies significantly between individual ice shelves both in absolute and relative magnitudes (Table 2). On average, observed ice thicknesses of the Ronne Filchner ice shelf are very close to hydrostatic, although the median *R* is -2.95 m. Two ice shelves, Dotson and Nickerson, have negative mean and median hydrostatic residuals, indicating that H_E underestimates the actual ice shelf thicknesses by about 1.0% and 3.3%, respectively. Larsen Ice Shelf has both the greatest absolute mean *R* of 26.7 m, and the greatest mean percent overestimation at 7.9%. Although the magnitudes of *R* for the Abbot and Getz ice shelves are similar, the mean percent overestimation is 4.2% for the thinner Abbot ice shelf and only 2.3% for the thicker Getz ice shelf. On average, observed ice thicknesses of West Antarctic ice shelves are 2.1% less than the hydrostatic thickness predicted from surface height.

Table 2. Overview of hydrostatic residual (R) and related statistics for all ice shelves. MAD = mean absolute deviation.

Shelf	# Campaigns	# Points	Mean *H* (m)	Mean *R* (m)	MAD of *R* (m)	Mean % difference between H_E and *H*
Ronne Filchner	21	421396	1056	0.0	16.6	0.8
Larsen	18	713041	339	26.7	25.4	16.3
George VI/ Wilkins/Stange	14	228589	288	7.3	12.6	24.3
Abbot	10	175580	266	11.1	15.6	11.8
PIG	18	273399	541	15.1	34.4	2.7
Thwaites	18	58961	531	18.7	49.2	3.6
Dotson/Crosson	17	103529	570	-5.6	27.3	-0.3
Getz	10	207276	483	11.3	21.2	2.0
Nickerson	4	22076	410	-13.3	21.7	-4.7
West Antarctica			**520**	**13.3**	**25.4**	**6.3**
Western Ross/McMurdo	12	89281	245	0.3	22.3	0.3
Drygalski/ Nordenskjold	4	4954	528	20.6	42.5	10.6
Cook	1	1979	605	27.7	15.1	4.8
Ninnis	2	2337	622	59.5	85.9	37.8
Mertz	3	1948	585	18.6	39.6	3.8
Astrolabe	1	254	506	-37.0	68.5	-5.7
Frost/Holmes	2	1695	475	48.4	56.1	8.2
Moscow University	6	13318	1000	33.2	56.2	3.5
Totten	19	102371	888	39.2	76.4	4.5
Vincennes Bay/ Underwood	16	5764	582	-23.7	104.0	11.2
Shackleton	5	10423	510	5.4	36.1	5.2
West	1	7839	495	15.4	21.1	2.9
East Antarctica (all shelves)			**603**	**20.3**	**54.4**	**1.4**
East Antarctica (3+ campaigns)			**608**	**19.9**	**55.3**	**3.1**
Overall (all shelves)			**529**	**14.0**	**28.2**	**5.8**
Overall (3+ campaigns)			**529**	**13.9**	**28.1**	**6.0**

For the twelve East Antarctic ice shelf systems with contemporaneous thickness and surface height measurements, the mean *R* is 17.3 m, or the observed thickness is 2.7% thinner ice than the estimated hydrostatic thickness. The density of observations is much lower in East

Antarctica than West Antarctica, and several ice shelves have coverage by only one or two campaigns. Thus, it is difficult to generalize results for most ice shelves, and mean and median R values vary more widely than on West Antarctic ice shelves (Table 2). Excluding the ice shelves with two or fewer campaigns (Cook, Ninnis, Astrolabe, Frost/Holmes, and West), the mean R is 13.4 m, corresponding to a 1.7% overestimation of hydrostatic ice thickness based on freeboard height. Our measurements of the Ross Ice Shelf, while dense, only cover its far western portion near McMurdo and the northernmost glaciers draining the Trans-Antarctic Mountains, so we term this region the Western Ross/McMurdo Ice Shelf system. While the mean value of R for this area is near zero at 0.3 m, the median value is -3.7 m, equivalent to observed thicknesses being 1.5% greater than hydrostatic. The Moscow University and Totten Glacier ice shelves were also surveyed with similar density as West Antarctic ice shelves. Of the East Antarctic ice shelves surveyed by three or more campaigns, Moscow University and Totten Glacier ice shelf region shows the largest disagreements between hydrostatic and measured thickness, but fairly low percent overestimations of ice thickness. Two ice shelf systems exhibit negative mean R values, including the single usable ground track on Astrolabe ice shelf, and the Vincennes Bay/Underwood ice shelf region, in which the hydrostatic assumption underestimates ice thickness by 7.3% and 4.1%, respectively. The other ice shelf regions with fewer than three campaigns (Cook, Ninnis, Frost/Holmes, and West) exhibit positive hydrostatic residuals. The disparities between densely and sparsely surveyed ice shelves indicate that there is high spatial variability within an ice shelf as well as among ice shelves.

Overall, over three-quarters of point estimates of H_E are within 10% of H, and just over half are within 5%, or 25 m. Histograms of both R and the percent misestimation have a positive skew, although the mode of R values for West Antarctica is positive, while the mode for East Antarctica is negative (Fig. 3). Notably, the mode for the percent difference is negative (between -2 and 0%) for West Antarctica, although it is positive (between 0 and 2%) for East Antarctica, and the mean and median for both ice sheets are positive (Fig. 1, Fig. 3).

4.2. Spatial Variability

4.2.1. Variability on 10+ kilometer scales

Disagreement between observed thickness and hydrostatic thickness varies widely within and among ice shelves, although a few patterns emerged. We sample several ground tracks in each ice shelf system to investigate spatial patterns in R (see Supplement). In general, over distances > 10 km, the hydrostatic assumption overestimates ice thickness where the ice is relatively thicker, and underestimates ice thickness where the ice is relatively thinner. Alternatively, the ice surface is elevated relative to the predicted flotation level where the ice is thicker and is depressed relative to flotation where the ice is thinner. Furthermore, R tends to increase with distance from the grounding line. The average R within 25 km of the grounding line is 11.3 m and the average R within 200 km of the grounding line is 14.0 m. Only the Ronne-Filchner and Larsen ice shelves have data >200 km from the grounding line (Fig. 4).

4.2.2. Grounding zones

On several ice shelves, the characteristic surface break-in-slope (Fricker and others, 2009) within 10 km of grounding lines is associated with a highly variable R along-track (Fig. 5). IPR ice thicknesses are generally less than hydrostatic near the grounding line and greater than hydrostatic at the local surface minima (Fig. 5a at 5 km and 122 km, Fig. 5b at ~1 km, Fig. 5c at ~0.5 km) or inflection point (Fig. 5c at 15 km) at the break-in-slope, which is often associated with a local thickness maximum. Where the surface height rebounds further along-track, observed thicknesses drop back below hydrostatic. Beyond the grounding line break-in-slope feature, however, variations in *R* are not necessarily similar along these ground tracks. For all sampled ground tracks with a sufficient number of measurements intersecting the grounding line, 72% show negative values for *R* coinciding with the break-in-slope. Cumulative average values for *R* decrease with increasing distance from the grounding line; mean *R* is 33.5 m for points within 1 km of the grounding line and 11.6 m for all points within 10 km of the grounding line (Fig. 5d), which is close to the mean *R* value for points within 25 km of the grounding line (Fig. 4).

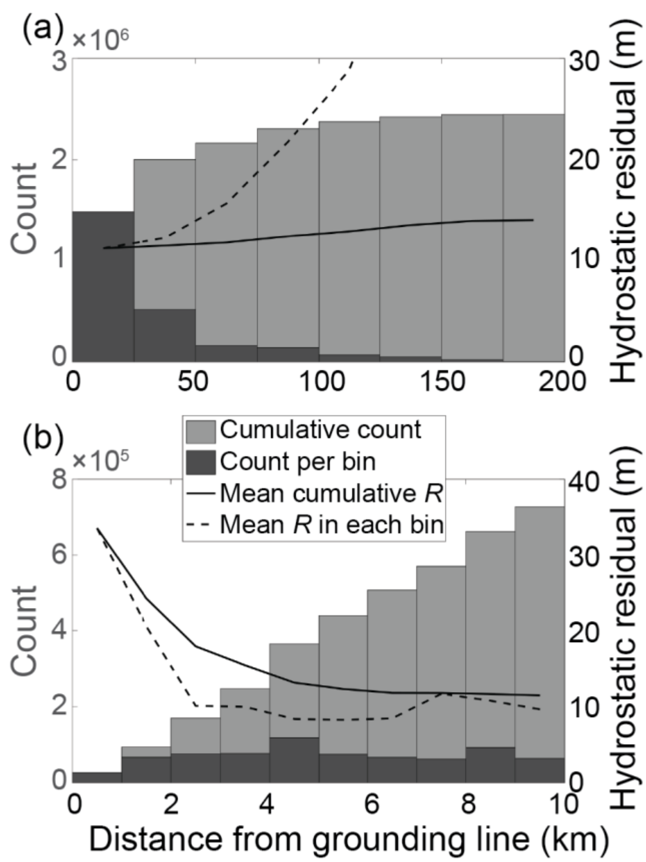

Figure 4. Left Y axis shows the cumulative (light gray) and bin total (dark gray) number of points within each successive distance from the grounding line (0 km). Right Y axis shows the mean *R* of all cumulative points (solid curve) and points within each bin (dashed curve) for each successive distance from the grounding line. (a) shows bins of 25 km; (b) shows bins of 1 km.

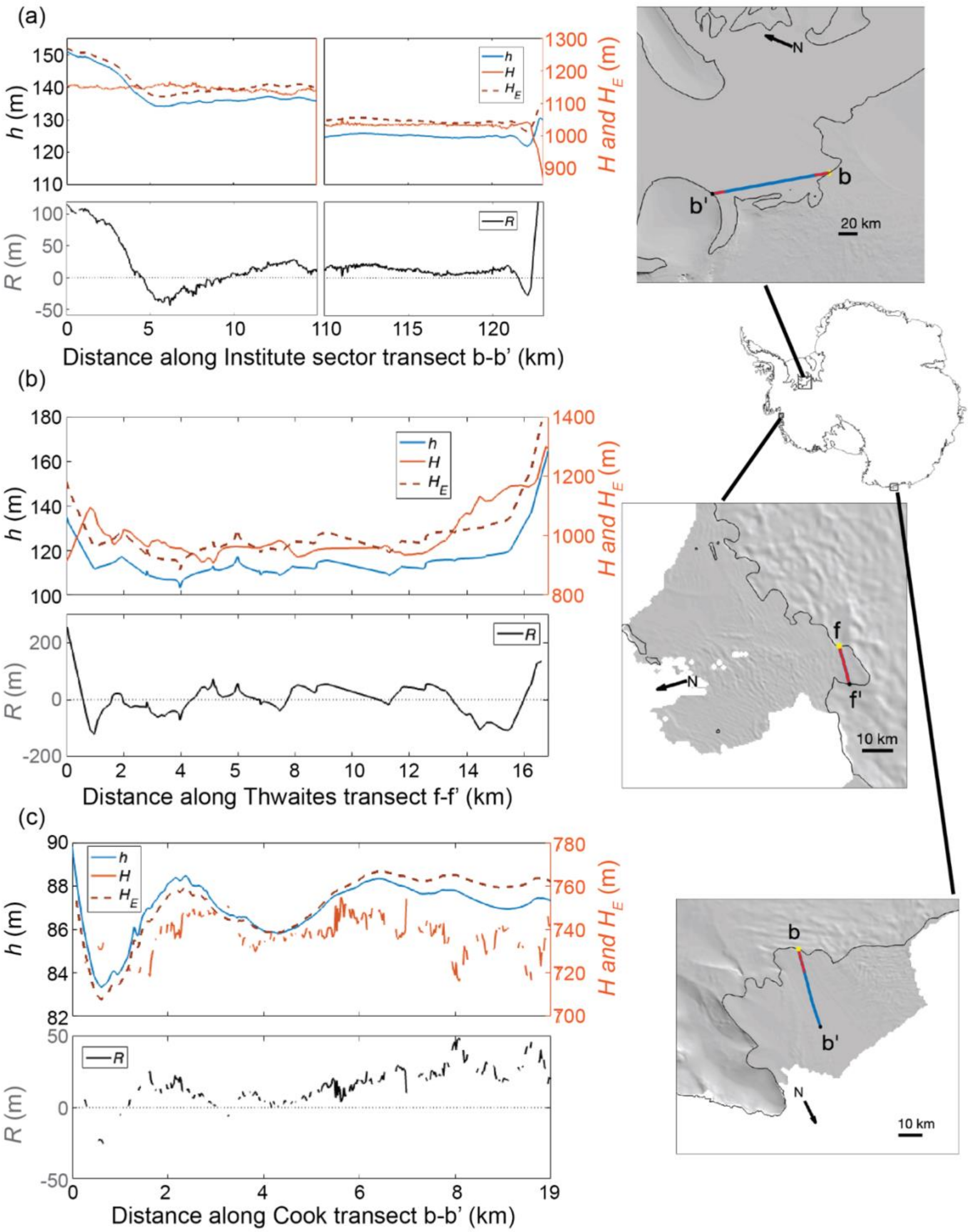

249 **Figure 5**. (a-c) Selected transects that start and/or end at a grounding line with a break-in-slope feature 1-5 km from the grounding line. Top panel of (a-c) shows surface height *h* (blue curve, left Y axis), IPR thickness *H* and hydrostatic thickness H_E (orange solid and red dashed curves, right Y axis), while the bottom panel shows hydrostatic residual *R*. Map insets show the location of each transect (a: transect b-b' downstream of Institute Ice Stream, b: transect f-f' on Thwaites Ice Shelf, and c: transect b-b' on Cook Ice Shelf), with plotted portions in (a-c) marked in orange.

4.2.3. Variability on kilometer scales

A pattern common to all ice shelves is that changes in R are generally inversely related to changes in H over distances <10 km, with some exceptions. This indicates that the surface topography is muted relative to the thickness profile, especially where peaks in observed thickness and surface height are associated with negative R values, and where local minima in observed thickness and surface height are associated with positive R values. However, sampled ground tracks also show that surface peaks and troughs aren't always aligned with variations in the thickness profile, and that there are some regions where the surface topography is exaggerated compared to the thickness profile. Fig. 6 shows examples of these patterns along transects from the Foundation ice stream sector of the Ronne-Filchner Ice Shelf, the Getz Ice Shelf, and the Totten Ice Shelf.

Two basal channels are intersected by the Foundation sector transect b-b', at 5-10 km and 20-24 km (Fig. 6a). Both basal channels exhibit a mismatch between surface slope and thickness gradient, leading to thinner ice than hydrostatic on the true right flank and thicker ice on the true left flank, with the mean also thicker than hydrostatic. This pattern is common to other basal channel intersections, such as those intersecting the Getz transect e-e' at 21-27 km and at 75-80 km (Fig. 6c) and the Totten transect e-e' at 7-11 km (Fig. 6b). However, some basal channels are thicker than hydrostatic at both flanks and thinner than hydrostatic within the channel, particularly when the surface trough and thickness minimum are aligned, such as those that intersect the Getz transect e-e' at 42-47 km (Fig. 6c) and the Totten transect e-e' at 15 -21 km and 23-27 km (Fig. 6b). Similar patterns can also be seen in other selected transects, shown and described in the Supplementary Material.

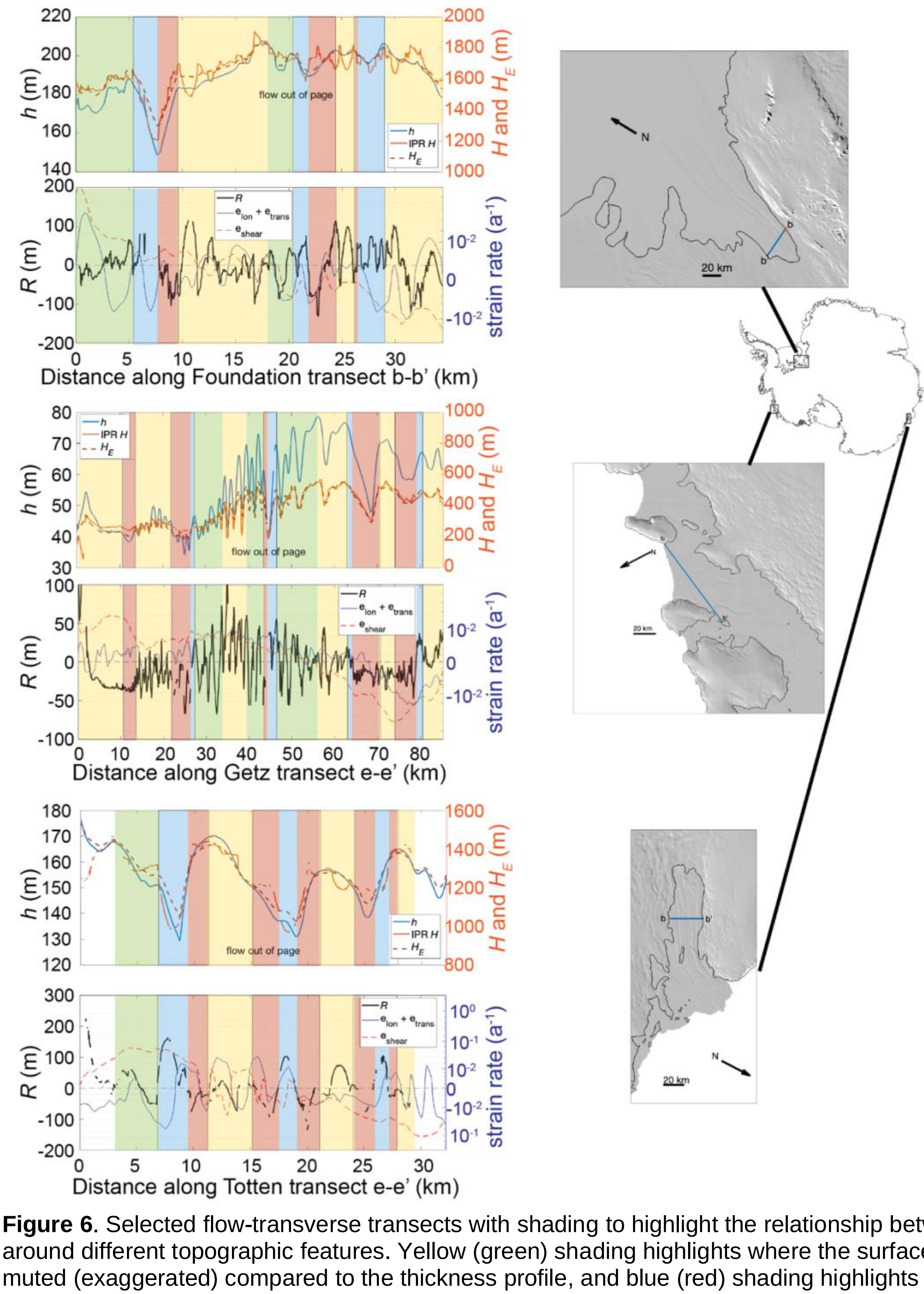

Figure 6. Selected flow-transverse transects with shading to highlight the relationship between H and H_E around different topographic features. Yellow (green) shading highlights where the surface topography is muted (exaggerated) compared to the thickness profile, and blue (red) shading highlights where the surface is too low (high) within large surface troughs/thin points (such as basal channels). Top panel of (a-c) shows surface height h (blue curve, left Y axis), IPR thickness H and hydrostatic thickness H_E (orange solid and red dashed curves, right Y axis), while the bottom panel shows hydrostatic residual R (black curve, left Y axis) and the sum of normal strain rates and the shear strain rates (solid blue and dashed red curves, right Y axis). Map insets show the location of each transect (a: MCoRDS transect b-b' on Ronne-Filchner ice shelf in the Foundation ice stream sector, b: HiCARS transect c-c' on Totten Ice Shelf, and c: MCoRDS transect e-e' on the Getz Ice Shelf).

5. DISCUSSION

5.1. Spatial variability in *R*

The spatial variability shown in our estimates of *R* is somewhat consistent with other studies, particularly near the grounding zone. Near the grounding line, we do not expect the ice to be freely floating because it is dynamically linked to the grounded ice and experiences flexure due to variations in sea level (e.g., tides) for several kilometers downstream of the true grounding line rather than simple vertical displacement (Rignot and others, 2011a; Friedl and others, 2020). The grounding line used in this study was identified from differential satellite radar interferometry data acquired in 2007-2009, and thus most closely represents the landward limit of tidal flexure (Mouginot and others, 2017; Rignot and others, 2013); much of the airborne thickness and altimetry data included in analysis is likely within the flexure zone, which often extends a few hundred meters to a few kilometers past the break-in-slope or surface minimum (Rignot and others, 2011a). The distance between the grounding line and the first seaward point at which the ice is freely floating depends on ice rheology, surface and basal topography, ice velocities and the thermal forcing of the ocean (Griggs and Bamber, 2011). Changes in ice properties may lead to decoupling between thickness and surface height gradients (Rignot and Jacobs, 2002), leading to high hydrostatic residuals. Griggs and Bamber (2011) showed that observed thickness measurements were up to 100 m lower than those obtained from ERS-1 surface heights within 10 km of the grounding line, while Chuter and Bamber (2015) found the opposite sign, largely due to a reduction in hydrostatic thicknesses as a result of the snow penetration and smoother data obtained from CryoSat-2 (which is unaffected by loss of lock, unlike ERS-1). Both studies found greater absolute hydrostatic residuals and standard deviations near grounding lines than over entire ice shelves, and attributed this to the breakdown of the hydrostatic assumption near the grounding zone due to vertical stresses associated with elastic bending and to greater uncertainties in firn thickness on the steep slopes within the grounding zone. Our results are more consistent with those of Griggs and Bamber, as the mean *R* within 10 km of the grounding line is consistently positive (Fig. 4b), although we do find negative *R* values associated with the break-in-slope of the surface profile within 10 km of the grounding line (Fig. 5). We concur that the hydrostatic assumption is unreliable near the grounding line, but our more detailed observations show that the ice is possibly freely floating at 6-8 km from the grounding line (Fig. 5).

Hydrostatic residuals may reflect uncertainties in the parameters used to calculate hydrostatic thickness and/or physical phenomena preventing the ice from floating freely. The flotation of an ice shelf is dependent on its geometry and velocity; stress transfer may bend the ice to be concave or convex, thus raising or lowering the ice column. Furthermore, estimates of hydrostatic thickness rely on the modeled firn air content, H_a, which is highly uncertain. Underestimation (overestimation) of the firn density would result in an overestimation (underestimation) of hydrostatic ice thickness based on its freeboard. Below, we discuss the measurement errors and uncertainties that may contribute to hydrostatic residuals, and we assess their impacts on basal melt rate estimates.

5.2. Confidence in ice penetrating radar thickness measurements

As stated in Section 3.1, our crossover analysis shows that radar thickness measurements were highly self-consistent. This indicates that hydrostatic residuals cannot be explained by thickness measurement errors, but it does not rule out the possibility that the MCoRDS or HiCARS thickness measurements are biased. Indeed, HiCARS ice thicknesses are reported to tend to be biased high based on a first return, and biased low based on a nadir return (Blankenship and others, 2011). Outliers likely represent steep thickness gradients near the intersections due to crevassing or other damage to the ice. Furthermore, shear heating in ice sheet shear margins has been associated with radar signal attenuation leading to dimmed basal echoes and absent or low-confidence radar picks (Summers and Schroeder, 2022), however our data show no clear relationship between missing or low-confidence radar picks and high shear strain rates.

5.3. Impact of ice column component thickness and density on hydrostatic imbalance

We do not assess the impact of accreted marine ice on the hydrostatic residual for the ice shelves in this study. Marine ice can have a density of up to 938 kg m^{-3} (Craven and others, 2009), so we expect that failure to consider accreted marine ice would lead to an underestimation of hydrostatic thickness since a denser ice column sits lower in the water column. Griggs and Bamber (2011) found that ice thickness was underestimated by 5% by not including marine ice (thereby underestimating ice density) in the upper-bound case where half of the total thickness is composed of marine ice. The presence of marine ice may also result in low-confidence picks for the ice shelf base due to its higher conductivity and radar wave energy absorption than meteoric ice (Vaňková and others, 2021). The thickness of marine ice has been estimated for several ice shelves, but few of these areas were surveyed in our dataset. On the Ronne-Filchner ice shelf, marine ice exceeding 100 m in thickness is expected north of 80 S (Vaňková and others, 2021), but most of our ground tracks fall south of this latitude. Marine ice up to 80 m thick is also expected along several flowlines on Larsen C ice shelf (Holland and others, 2009; Harrison and others, 2022), but these regions are not associated with anomalous R values.

Uncertainty in the thickness and density of firn may contribute to hydrostatic residuals. We approximate how these parameters would need to change for the measured H and h to satisfy the hydrostatic assumption. When referring to the firn air column thickness and density necessary to satisfy the hydrostatic assumption, we will denote them with the subscript E for consistency with H_E.

Because R is generally positive, the ice must be less dense than we assume for the measured thickness and surface to be in hydrostatic equilibrium. This disparity in densities could be a result of uncertainties in the modeled firn air column thickness H_a and/or assumed density ρ_a. To independently investigate the thickness (H_{aE}) or density (ρ_{aE}) of the firn air column needed to account for R, we differentiate Eqn (1) with respect to both quantities:

$$\frac{dH}{dH_{aE}} = \frac{\rho_a - \rho_i}{\rho_i - \rho_w} = 8.4 \qquad (3a)$$

$$\frac{dH}{d\rho_{aE}} = \frac{H_a}{\rho_i - \rho_w}. \qquad (3b)$$

Substituting R = dH, we calculate dH_a (the difference between H_{aE} and H_a), assuming ρ_a = 2 kg m^{-3} is simply:

$$dH_a = \frac{R}{8.4}\,, \qquad (4a)$$

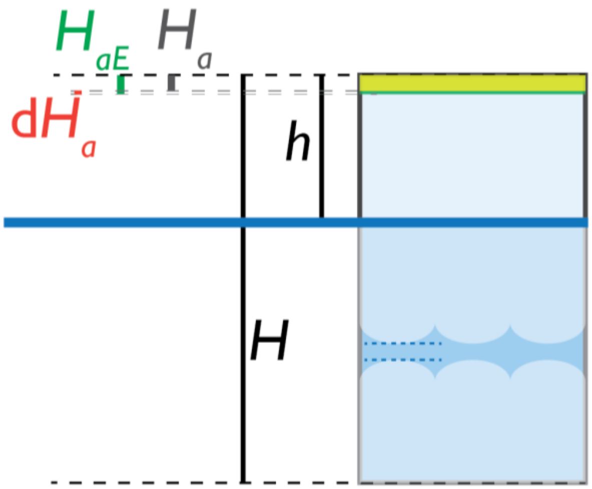

Figure 8. Cartoon graphic showing relevant quantities for a column of ice floating in seawater. The ice below sea level is discontinuous to exaggerate the vertical scale. Quantities represent observed or accepted values as in Fig. 2, with added H_{aE}, which is the firn air column thickness necessary to bring the observed ice column into hydrostatic equilibrium, and dH_a, which is the difference between H_{aE} and the modeled firn air column thickness H_a.

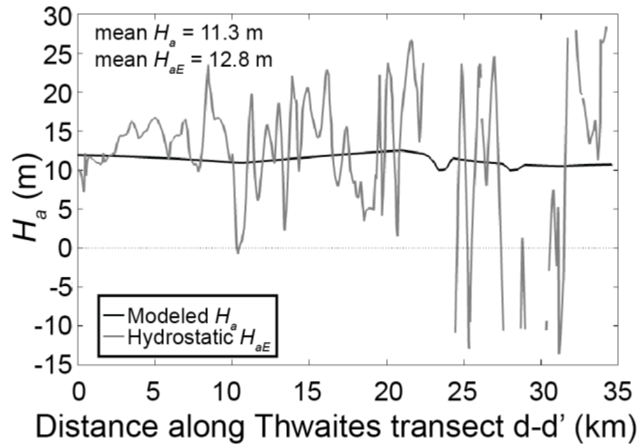

Figure 7. Thwaites transect d-d' showing modeled H_a (black curve), and H_{aE} (gray curve).

and the dρ_a (the difference between ρ_{aE} and ρ_a), assuming modeled firn air column thickness H_a is correct, and that ρ_i = 918 kg m^{-3} and ρ_s = 1027 kg m^{-3}, is

$$d\rho_a = \frac{R(\rho_i - \rho_s)}{H_a} = \frac{-109 * R}{H_a}. \qquad (4b)$$

Eqn (4a) shows that when R is positive (negative), dH_a must also be positive (negative) so that the ρ_a = 2 kg m^{-3} accounts for more (less) of the total thickness of the ice shelf, decreasing (increasing) the vertically averaged column density to flotation. A thicker firn-air column would account for the higher observed h required for the observed H to satisfy the hydrostatic assumption, because it would lower the density of the observed ice column, forcing it to float higher in the water (i.e., higher freeboard, smaller submerged portion than if the ice column were denser; Fig. 7). In reality, a thicker firn air column indicates a deeper firn layer (Ligtenberg and others, 2011). Similarly, if we assume that the modeled firn-air column thickness is correct but that the density is unknown, Eqn (4b) shows that when R is positive (negative), dρ_a must be negative (positive) in order to bring the vertically averaged column density down (up).

Overall, the mean dH_a is within the nominal 10 m uncertainty of the firn model (Ligtenberg and others, 2011; Ligtenberg and others, 2014), but this uncertainty is poorly constrained spatially. Indeed, a dH_a of ± 10 m would result in an R of ± 84 m, and our R values exceed ± 84 m in several places (Fig. 5, Fig. 6), even resulting in negative hydrostatic firn air column thicknesses (H_{aE}) over short distances (e.g., Fig. 8). Furthermore, the direct relationship between dH_a and R means that the firn-air column thickness would vary widely over the same spatial scales as the hydrostatic residual. This is unlikely, particularly where the surface is relatively flat (Fig. 4, Fig. 6, Fig. 8), since the spatial variability in H_a is driven primarily by surface climatic conditions, which do not vary on sub-km scales (Lenaerts and others, 2012; Ligtenberg and others, 2011; Ligtenberg and others, 2014). Our results show that regions like Remnant Larsen B, and near the Bawden ice rise on Larsen C require a > 10 m deeper firn layer than modeled to satisfy the hydrostatic assumption, despite absent or near zero modeled and observed firn thicknesses in this region (Holland and others, 2011; Ligtenberg and others, 2011).

The mean d$\boldsymbol{\rho}_a$ would result in unphysical mean hydrostatic firn air column densities ($\boldsymbol{\rho}_{aE}$) for all but five ice shelves, indicating that uncertainties in accounting for the firn air column alone cannot explain R (Table S2). Only the Ronne Filchner ice shelf is well-constrained, on average, by assumed $\boldsymbol{\rho}_a$ and modeled H_a values, pointing to the need for more observations of firn properties and firn densification models of higher confidence. Larsen C has the most negative d$\boldsymbol{\rho}_a$ ($\boldsymbol{\rho}_{aE}$ = -1659 kg m^{-3}) required for balance, providing further evidence that the measured surface is much too high for ice of the observed thickness to be in hydrostatic equilibrium.

5.4. Relationship between *R* and strain rates

If hydrostatic balance may partly be due to the transfer of vertical stress (i.e., stress bridging) within the ice shelf, we expect that R will also be related to strain rates (Cuffey and Paterson, 2010). We estimate longitudinal (e_{lon}), transverse (e_{trans}) and shear (e_{shear}) surface strain rates from the NASA MEaSUREs InSAR-derived average velocity map (Mouginot and others, 2012; Rignot and others, 2011b, 2017) following the approach of Bindschadler and others (1996) at each measurement point. The relationships between R and the median $\nabla\cdot u = e_{lon} + e_{trans}$ (normal strain rates, where ∇ is the del operator and u is velocity) and absolute value of e_{shear} within 1 m increments of R are plotted in Fig. 9. We find that, as expected, low-magnitude R values coincide with low strain rates, and R becomes more negative with increasing shear and normal strain rates. A negative R means the ice is thicker than hydrostatic (the surface is lower than flotation), which is consistent with increased vertical stress due to bridging (Le Brocq and others, 2013; Drews, 2015). Increasing R does not correlate with shear except for very high values. Normal strain rates increase with both positive and negative R, which may depend on the direction of stress transfer. However, the median $\nabla\cdot u$ appears to have an upper limit of ~2.5x10^{-3} a^{-1} for R values > 50 m.

The relationship between R and $\nabla\cdot u$ described above (Fig. 9a) is dominated by West Antarctic ice shelves (Fig. 9b). However, individual ice shelves show significant variability (Figs. S43-S44). Specifically in West Antarctica, we see that strain rates tend to decrease with increasing R > 50 m, a pattern also found at Ronne Filchner, Larsen C, and George VI/Wilkins/Stange, Abbot, and Dotson/Crosson ice shelves (Fig. S43a-d, g). Between R values of -50 to 50 m, the near-zero and negative strain rates exhibited in Fig. 9a are reflected in the plots for all ice shelves except Larsen C and Thwaites, which are entirely extensional (Fig. S43). For R values below -50 m, increasing strain rates with decreasing R are most prevalent on PIG, Thwaites, Dotson, and Getz ice shelves (Fig. S43e-h).

For East Antarctic ice shelves, excluding the western Ross Ice Shelf/McMurdo ice shelf system, the median $\nabla\cdot u$ is positive for all values of R, with higher magnitudes of R generally correlating with $\nabla\cdot u$ (Fig. 9b). This is generally reflected on all East Antarctic ice shelves (Fig. S44a-l), and particularly for the Totten ice shelf (Fig. S44i). However, all ice shelves except for the Frost/Holmes, Totten, and Vincennes Bay/Underwood ice shelves show compressive strain rates associated with seemingly random values of R. On the western Ross/McMurdo Ice Shelf system, *R* values near zero tend to occur in areas with highly compressive strain rates, and near-zero strain rates are associated with *R* values > |50| m (Fig. S44a).

In summary, we find that smaller hydrostatic imbalances tend to be associated with compression, while larger imbalances, particularly positive *R* values, are more likely to be associated with extension. However, this general pattern is not consistent at the scale of individual ice shelves (Figs. S43-S44).

There is no clear relationship between shear strain rates and positive *R* values for the whole dataset, but more negative *R* values are associated with higher shear strain rates (Fig. 9a, c). This signal is also dominated by West Antarctic ice shelves. Individual West Antarctic ice shelves Ronne Filchner, PIG, Thwaites, Getz, and Nickerson also show consistently increasing shear strain rates with increasing *R* values > 0 (Fig. S43a, e, f, h, i). In East Antarctica, median shear strain rates tend to increase as *R* becomes more negative (Fig. S44b-l), except for on the western Ross/McMurdo ice shelf system, where shear strain rates are low where *R* is high, and high where *R* is low (Fig. S44a). This result, however, may be due to the sparse data density over areas where we might expect high *R* values on the western Ross/McMurdo ice shelf system. We would expect more negative *R* values in areas of higher shear as shear stresses may be transferred horizontally from the interior of the ice sheet to the margin.

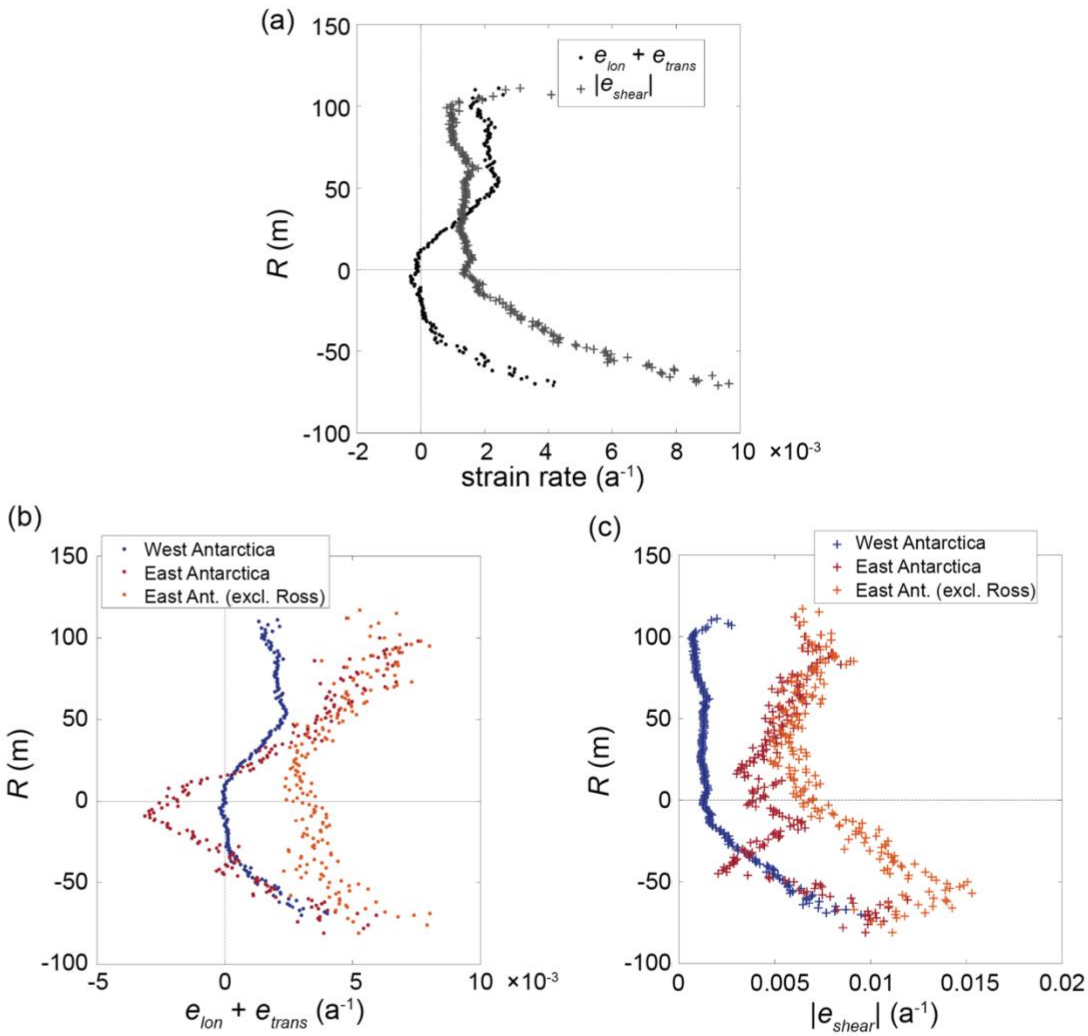

Figure 9. (a) Median normal strain rates (e_{lon} + e_{shear}, black dots) and absolute values of shear strain rates ($|e_{shear}|$, gray + signs) for points within bins of 1 m increments of *R* for all radar points. (b) and (c) show median e_{lon} + e_{trans} and $|e_{shear}|$, respectively, within bins of 1 m increments of *R* for West Antarctica (blue dots and + signs), East Antarctica (all shelves, red dots and + signs) and East Antarctic shelves excluding the Western Ross/McMurdo ice shelf region (orange dots and + signs). Bins containing fewer than the 40th percentile of N (1100 points for (a)) were excluded.

5.5. Impact of *R* on estimates of basal melt/accretion rates

The over/underestimation of the rate of basal mass change is dependent on the signs of *R* and the strain rates. Because *R* and median strain rates for the vast majority of points are near zero (Fig. 9), we expect that the basal mass change estimated from hydrostatic thickness, M_{bE}, won't be greatly misestimated. Assuming incompressibility of ice, and following the continuity approach, the basal mass balance is estimated as (e.g., Dutrieux and others 2013; Berger and others, 2017; Shean and others, 2019; Chartrand and Howat, 2020):

$$M_b = \left(\frac{DH}{Dt} + H(\nabla \cdot u)\right)\frac{\rho_i}{\rho_w} - M_s, \tag{5}$$

where M_b is the rate of basal mass loss/gain in m w.e. a^{-1} (meters of freshwater equivalent per year) and is positive for refreezing and negative for basal melt, M_s is the surface ablation/accumulation rate, which is positive for mass gain, ∇ is the del operator, u is the column-average horizontal velocity of the ice (m a^{-1}), and ρ_w is the density of freshwater, 1,000 kg m^{-2}. The density of ice is assumed to be 918 kg m^{-3}. The subscript E is used to denote the calculation of basal mass balance using the hydrostatic assumption. Estimates of basal mass balance from spaceborne surface height measurements, such as those from Adusumilli and others (2020) rely on the calculation of H_E, and we will thus refer to these estimates as M_{bE}.

To examine the impact of the hydrostatic residual on mass balance rates estimated from freeboard height, we substitute H_E - R in for H (Eqn (2)) in Eqn (5) and differentiate with respect to R, assuming R is constant in time:

$$\frac{dM_b}{dR} = -(\nabla \cdot u)\frac{\rho_i}{\rho_w}, \tag{6}$$

so that the magnitude and sign of sensitivity of estimated basal mass balance rate to hydrostatic imbalance is dependent on the strain rate. We then multiply by Eqn (6) by R to calculate dM_b at each point:

$$dM_b = -R\left((\nabla \cdot u)\frac{\rho_i}{\rho_w}\right). \tag{7a}$$

Substituting H_E - H back in for R, we get

$$dM_b = -(H_E - H) * (\nabla \cdot u)\frac{\rho_i}{\rho_w} = (H - H_E) * (\nabla \cdot u)\frac{\rho_i}{\rho_w}. \tag{7a}$$

We estimate $\nabla \cdot u$ as described in Section 5.3. We then compare dM_b with basal mass balance rates obtained from the ICESat and ICESat-2 satellite record (Adusumilli and others, 2020), termed M_{bE}. Eqns (7) show that dM_b will have the opposite sign as R if the ice is extending ($\nabla \cdot u$ > 0), and the same sign as R if the ice is compressing ($\nabla \cdot u$ < 0). In other words, where R is positive (thickness is overestimated), M_{bE} will be too positive where strain rates are tensile (dM_b < 0) and too negative where strain rates are compressive (dM_b > 0). Where R is negative (thickness is underestimated), M_{bE} will be too negative where strain rates are tensile (dM_b < 0) and too positive where strain rates are compressive (dM_b > 0). These interpretations are also summarized in Box 1. These relationships hold at each ground track coordinate, but not necessarily for the aggregated ice shelf results (Table S3). We divide the absolute value of dM_b by M_{bE} from the satellite record and multiply by 100 to obtain a percent difference (Table S3) of mass balance estimates.

Box 1. Impact of *R* on basal mass balance estimates

	Extension $\nabla \cdot u > 0$	Compression $\nabla \cdot u < 0$
R > 0 $DH/Dt = 0$ $M_s = 0$	$dM_b < 0$ M_{bE} too positive $0 < M_b < M_{bE}$	$dM_b > 0$ M_{bE} too negative $M_{bE} < M_b < 0$
R < 0 $DH/Dt = 0$, $M_s = 0$	$dM_b > 0$ M_{bE} too negative $0 < M_{bE} < M_b$	$dM_b < 0$ M_{bE} too positive $M_b < M_{bE} < 0$

Overall, accounting for R results in a ~0.2% difference from the median rate of basal mass change calculated in Adusumilli and others (2020). Since strain rates of ice shelves tend to be on the order of 10^{-3} per year, this aligns with our expectation that the impact of R on M_b is generally small. However, hydrostatic imbalance may introduce a bias that, when integrated over large areas, may be significant to the total mass balance. Also, the impact may be significant in areas of high strain rates, such as at shear margins, or in areas of high R, such as basal channels. Overall, the mean (median) $|dM_b|$ for all data points is 0.19 (0.01) ± 1.4 m w.e. a^{-1}, meaning that on average, the hydrostatic assumption over- or underestimates basal melt rates by ~0.2 m w.e. a^{-1}, depending on the flow regime. This is an order of magnitude smaller than the median uncertainty in basal mass balance calculated by Adusumilli and others (2020; ± 1.1 m w.e. a^{-1}). However, the impact of R on basal mass change rate estimates varies between ice shelves, and on local scales (Table S3). The most extreme impacts on median dM_b occur on the small ice shelves of East Antarctica, such as the Cook ice shelf (dM_b = -0.15 ± 0.23 m w.e. a^{-1}), the Ninnis ice shelf (dM_b = -0.44 ± 2.52 m w.e. a^{-1}), Astrolabe ice shelf (dM_b = 0.75 ± 2.81 m w.e. a^{-1}) and the Porpoise Bay ice shelf region (dM_b = -0.41 ± 3.40 m w.e. a^{-1}). When compared to the median melt rates from Adusumilli and others (2020; bilinearly interpolated to ground track coordinates), however, the most extreme relative impacts on basal mass balance were on Larsen C, where we find that M_{bE} is overestimated by ~2.8% (so that the actual M_b is more negative/more melt is occurring than is accounted for by the hydrostatic assumption), Cook Ice Shelf, where M_{bE} is overestimated by ~15.6%, the Porpoise Bay region, where M_{bE} is overestimated by ~3.3%, and West Ice Shelf, where M_{bE} is overestimated by ~4.8%. The dM_b values of the latter three ice shelves are likely dominated by extreme R values due to the relatively low number of ground tracks in those regions.

Our results showing high magnitudes of R near basal channels and other potentially destabilizing features are consistent with other observations (e.g., Chartrand and Howat, 2020; Drews 2015; Dow and others, 2021) and point to the need for more detailed measurements near these features to accurately account for them in mass balance estimates. Hydrostatic imbalance has been shown to change over time as ice advects over an actively incising basal channel (Chartrand and Howat, 2020), indicating that repeat surface height measurements may yield erroneous basal melt rates. Although temporal analysis of R is not a goal of this study, several ground tracks with repeat coverage show that R changes over time at a variety of ice shelf features (Figs. S5, S6, S11, S12, S23-25, S38). Furthermore, analyses on the Roi Baudoin and Nansen Ice shelves have shown that satellite-derived surface velocities and related strain rates may be better suited to characterize basal feature morphology than the hydrostatic assumption (Drews, 2015; Dow and others, 2021). However, these studies used near-contemporaneous surface velocities to test the agreement between strain-rate and IPR-derived morphology, which are not widely available for supplementing hydrostatic calculations of ice thickness prior to the epoch of widespread availability of high-resolution speed and surface elevation data, such as from the GO_LIVE/ITS_LIVE and REMA projects (Fahnestock and others, 2015; Gardner and others, 2018; Noh and Howat, 2019).

Similarly, short-term and short-spatial-scale surface elevation changes are largely unrelated to basal mass balance and, if not accounted for, can lead to magnification of errors in estimating changes in ice thickness (Vaňková and Nicholls, 2022). Our results corroborate the assertion that errors in basal melt rates derived from satellite data (e.g., Adusumilli and others, 2020) are not spatially uniform (Vaňková and Nicholls, 2022), because R is not uniform in time or space, imparting unknown and potentially large errors in basal melt rates estimated from surface elevation.

6. CONCLUSIONS

We completed the first, large-scale comparison between thickness observed from ice-penetrating radar and the hydrostatic thickness estimated from contemporaneous surface elevation measurements over Antarctic ice shelves. Using MCoRDS/HiCARS ice penetrating radar and ATM/Riegl laser altimetry, we have found that Antarctic ice shelves are, on average, about 13 m (2%) thinner than hydrostatic thickness. However, the mean hydrostatic residual, or the difference between estimated and observed thickness, R, varies among individual ice shelf systems and can vary by 100s of meters over sub-kilometer scales. The greatest hydrostatic residuals in West Antarctica are found on the Larsen C ice shelf, where the measured thickness is ~27 m, or 8%, less than hydrostatic. Of the East Antarctic ice shelves with similar data density to West Antarctica, the greatest residuals are found on Moscow University and Totten Ice Shelves (R = 33, or 3%, and R = 39, or 4%, respectively), although the ice shelves with three or fewer campaigns also have high magnitude R values, reaching 59 m, or 10%, on the Ninnis ice shelf. We expect that the sparse coverage on these shelves allows extreme values to dominate the mean hydrostatic residual.

On kilometer scales, few spatial patterns in hydrostatic residual are apparent. Most notably, the break-in-slope feature within 10 km of the grounding line is often associated with negative R values, and the mean R decreases (but remains above zero) with increasing distance from the grounding line up to 10 km. Past 25 km, the mean R increases with increasing distance from the grounding line. We also find that hydrostatic thickness sometimes exaggerates thickness anomalies compared to the measurements, and sometimes mutes thickness anomalies, including for surface and basal crevasses and basal channels.

We assess whether measurement errors, uncertainties in firn thickness and/or density could account for the average hydrostatic residuals. A crossover analysis of same-campaign thickness measurements shows high consistency in both MCoRDS and HiCARS data, and low errors are expected for surface elevation measurements. On average, R can largely be corrected by assuming a lower vertically averaged density for ice shelves. This can be achieved physically by accounting for a negative bias in the modeled firn air column thickness. However, the variability in *R* across sub-kilometer scales cannot be explained by measurement errors or assumed firn properties. We posit that higher spatial resolutions and accuracies in firn column observations and densification models are needed for confidence in estimating hydrostatic thickness.

Furthermore, although most *R* values and strain rates are near zero, higher shear and normal strain rates are associated with $|R| > 50$ m, which is consistent with the concept of stress bridging where the hydrostatic thickness is less than the measured thickness (i.e., vertical stress transfer may hold the surface below its hydrostatic height). However, on small scales, strain rates do not correlate with *R*. One of the greatest implications of uncertainties in estimating hydrostatic thickness is that it will lead to uncertainties in estimating basal mass balance. Few studies consider thickness gradients across flow when modeling ice shelf flow and mass balance, yet we show that *R* has substantial implications for flow-transverse ice shelf dynamics, particularly on small scales. By isolating the impact of hydrostatic residual on basal mass balance, we find that overall, the hydrostatic assumption overestimates the rate of mass gain by 2%, but this varies spatially, depending on strain rates and thickness gradients. Furthermore, sampled repeat ground tracks show that *R* can change over time (in an Eulerian framework), pointing to the need for greater utilization of available thickness data and future thickness measurements, which will in turn improve estimates of hydrostatic thickness over time as well as spatially.

SUPPLEMENTARY MATERIAL. The supplementary material for this article can be found at (article web page).

ACKNOWLEDGEMENTS. Allison Chartrand was supported by NASA Future Investigators in NASA Earth and Space Science and Technology (FINESST) grant 80NSSC_20K1658 and the Distinguished University Fellowship at The Ohio State University. Ian Howat was supported by National Science Foundation Office of Polar Programs Grant 2217574. All IceBridge, ICECAP, and MEaSUREs airborne and geophysical data were obtained from NSIDC.

REFERENCES

Adusumilli S, Fricker HA, Medley B, Padman L and Siegfried MR (2020) Interannual variations in meltwater input to the Southern Ocean from Antarctic ice shelves. *Nature Geoscience* **13**(9), 616–620. doi:10.1038/s41561-020-0616-z.

Alley KE, Scambos TA, Alley RB and Holschuh N (2019) Troughs developed in ice-stream shear margins precondition ice shelves for ocean-driven breakup. *Science Advances* **5**(10), eaax2215. doi:10.1126/sciadv.aax2215.

Andersen OB and 8 others (2018) Improving the Coastal Mean Dynamic Topography by Geodetic Combination of Tide Gauge and Satellite Altimetry. *Marine Geodesy* **41**(6), 517–545. doi:10.1080/01490419.2018.1530320.

Andersen, OB and Knudsen, P (2009) DNSC08 mean sea surface and mean dynamic topography models. *Journal of Geophysical Research: Oceans* **114**(C11). doi:10.1029/2008JC005179.

Bamber J and Bentley CR (1994) A comparison of satellite-altimetry and ice-thickness measurements of the Ross Ice Shelf, Antarctica. *Annals of Glaciology* **20**, 357–364. doi:10.3189/1994AoG20-1-357-364.

Berger S, Drews R, Helm V, Sun S and Pattyn F (2017) Detecting high spatial variability of ice shelf basal mass balance, Roi Baudouin Ice Shelf, Antarctica. *The Cryosphere* **11**(6), 2675–2690. doi:10.5194/tc-11-2675-2017.

Bindschadler R and 17 others (2011) Getting around Antarctica: New high-resolution mappings of the grounded and freely-floating boundaries of the Antarctic ice sheet created for the International Polar Year. *The Cryosphere*. doi:https://doi.org/10.5194/tc-5-569-2011.

Bindschadler R, Vornberger P, Blankenship D, Scambos T and Jacobel R (1996) Surface velocity and mass balance of Ice Streams D and E, West Antarctica. *Journal of Glaciology* **42**(142), 461–475. doi:10.3189/S0022143000003452.

Blankenship, D and 12 others (2012a) IceBridge HiCARS 2 L2 Geolocated Ice Thickness, Version 1. doi:10.5067/9EBR2T0VXUDG.

Blankenship, D and 8 others (2012b) IceBridge Riegl Laser Altimeter L2 Geolocated Surface Elevation Triplets, Version 1. doi:10.5067/JV9DENETK13E.

Blankenship, D and 12 others (2011) IceBridge HiCARS 1 L2 Geolocated Ice Thickness, Version 1. doi:10.5067/F5FGUT9F5089.

Chartrand AM and Howat IM (2020) Basal Channel Evolution on the Getz Ice Shelf, West Antarctica. *Journal of Geophysical Research: Earth Surface* **125**(9), e2019JF005293. doi:10.1029/2019JF005293.

Chuter SJ and Bamber JL (2015) Antarctic ice shelf thickness from CryoSat-2 radar altimetry. *Geophysical Research Letters* **42**(24), 10,721-10,729. doi:10.1002/2015GL066515.

Craven M, Allison I, Fricker HA and Warner R (2009) Properties of a marine ice layer under the Amery Ice Shelf, East Antarctica. *Journal of Glaciology* **55**(192), 717–728. doi:10.3189/002214309789470941.

Dow CF and 9 others (2021) The complex basal morphology and ice dynamics of Nansen Ice Shelf, East Antarctica. *The Cryosphere Discussions*, 1–20. [preprint], doi:10.5194/tc-2021-168.

Drews R and 6 others (2016) Constraining variable density of ice shelves using wide-angle radar measurements. *The Cryosphere* **10**(2), 811–823. doi:10.5194/tc-10-811-2016.

Drews R (2015) Evolution of ice-shelf channels in Antarctic ice shelves. *The Cryosphere* **9**, 1169. doi:10.5194/tc-9-1169-2015.

Dutrieux P and 6 others (2013) Pine Island glacier ice shelf melt distributed at kilometre scales. *The Cryosphere* **7**(5), 1543–1555. doi:10.5194/tc-7-1543-2013.

Fahnestock M, Scambos T, Moon T, Gardner A, Haran T and Klinger M (2016) Rapid large-area mapping of ice flow using Landsat 8. *Remote Sensing of Environment* **185**, 84–94. doi:10.1016/j.rse.2015.11.023.

Förste C and 8 others (2014) EIGEN-6C4 The latest combined global gravity field model including GOCE data up to degree and order 2190 of GFZ Potsdam and GRGS Toulouse., 55102156 Bytes, 3 Files. doi:10.5880/ICGEM.2015.1.

Fricker HA, Coleman R, Padman L, Scambos TA, Bohlander J and Brunt KM (2009) Mapping the grounding zone of the Amery Ice Shelf, East Antarctica using InSAR, MODIS and ICESat. *Antarctic Science* **21**(5), 515–532. doi:10.1017/S095410200999023X.

Friedl P, Weiser F, Fluhrer A and Braun MH (2020) Remote sensing of glacier and ice sheet grounding lines: A review. *Earth-Science Reviews* **201**, 102948. doi:10.1016/j.earscirev.2019.102948.

Gardner AS and 6 others (2018) Increased West Antarctic and unchanged East Antarctic ice discharge over the last 7 years. *The Cryosphere* **12**(2), 521–547. doi:10.5194/tc-12-521-2018.

Griggs JA and Bamber JL (2011) Antarctic ice-shelf thickness from satellite radar altimetry. *Journal of Glaciology* **57**(203), 485–498. doi:10.3189/002214311796905659.

Harrison LC, Holland PR, Heywood KJ, Nicholls KW and Brisbourne AM (2022) Sensitivity of Melting, Freezing and Marine Ice Beneath Larsen C Ice Shelf to

Changes in Ocean Forcing. *Geophysical Research Letters* **49**(4), e2021GL096914. doi:10.1029/2021GL096914.

Holland PR and 6 others (2011) The air content of Larsen Ice Shelf. *Geophysical Research Letters* **38**(10). doi:10.1029/2011GL047245.

Holland PR, Corr HFJ, Vaughan DG, Jenkins A and Skvarca P (2009) Marine ice in Larsen Ice Shelf. *Geophysical Research Letters* **36**(11). doi:10.1029/2009GL038162.

Howat I and 17 others (2022) The Reference Elevation Model of Antarctica - Mosaics, Version 2. doi:10.7910/DVN/EBW8UC.

Howat IM, Porter C, Smith BE, Noh M-J and Morin P (2019) The Reference Elevation Model of Antarctica. *The Cryosphere* **13**(2), 665–674. doi:https://doi.org/10.5194/tc-13-665-2019.

Jackett DR and McDougall TJ (1997) A Neutral Density Variable for the World's Oceans. *Journal of Physical Oceanography* **27**(2), 237–263. doi:10.1175/1520-0485(1997)027<0237:ANDVFT>2.0.CO;2.

Le Brocq AM and 10 others (2013) Evidence from ice shelves for channelized meltwater flow beneath the Antarctic Ice Sheet. *Nature Geoscience* **6**(11), 945–948. doi:10.1038/ngeo1977.

Lenaerts JTM and 11 others (2014) High variability of climate and surface mass balance induced by Antarctic ice rises. *Journal of Glaciology* **60**(224), 1101–1110. doi:10.3189/2014JoG14J040.

Ligtenberg SRM, Kuipers Munneke P and van den Broeke MR (2014) Present and future variations in Antarctic firn air content. *The Cryosphere* **8**(5), 1711–1723. doi:https://doi.org/10.5194/tc-8-1711-2014.

Ligtenberg SRM, Helsen MM and Broeke MR van den (2011) An improved semi-empirical model for the densification of Antarctic firn. *The Cryosphere* **5**(4), 809–819. doi:https://doi.org/10.5194/tc-5-809-2011.

MacGregor JA and 45 others (2021) The Scientific Legacy of NASA's Operation IceBridge. *Reviews of Geophysics* **59**(2), e2020RG000712. doi:10.1029/2020RG000712.

MacGregor JA and 11 others (2015) Radar attenuation and temperature within the Greenland Ice Sheet. *Journal of Geophysical Research: Earth Surface* **120**(6), 983–1008. doi:10.1002/2014JF003418.

Martin C and 6 others (2012) Airborne Topographic Mapper Calibration Procedures and Accuracy Assessment. 20120008479. National Aeronautics and Space Administration, Washington, D. C. https://ntrs.nasa.gov/archive/nasa/casi.ntrs.nasa.gov/20120008479.pdf.

Medley B and 14 others (2014) Constraining the recent mass balance of Pine Island and Thwaites glaciers, West Antarctica, with airborne observations of snow accumulation. *The Cryosphere* **8**(4), 1375–1392. doi:10.5194/tc-8-1375-2014.

Morlighem M and 36 others (2020) Deep glacial troughs and stabilizing ridges unveiled beneath the margins of the Antarctic ice sheet. *Nature Geoscience* **13**(2), 132–137. doi:10.1038/s41561-019-0510-8.

Mouginot J, Scheuchl B and Rignot E (2012) Mapping of Ice Motion in Antarctica Using Synthetic-Aperture Radar Data. *Remote Sensing* **4**(9), 2753–2767. doi:10.3390/rs4092753.

Mouginot J, Scheuchl B and Rignot E (2017) MEaSUREs Antarctic Boundaries for IPY 2007-2009 from Satellite Radar, Version 2. doi:10.5067/AXE4121732AD.

Noh M-J and Howat IM (2019) Applications of High-Resolution, Cross-Track, Pushbroom Satellite Images With the SETSM Algorithm. *IEEE Journal of Selected Topics in Applied Earth Observations and Remote Sensing* **12**(10), 3885–3899. doi:10.1109/JSTARS.2019.2938146.

Paden JD, Li J, Leuschen C, Rodriguez-Morales F and Hale R (2011) Pre-IceBridge MCoRDS L2 Ice Thickness, Version 1. https://nsidc.org/data/brmcr2/versions/1.

Paden J, Li J, Leuschen C, Rodriguez-Morales F and Hale R (2010) IceBridge MCoRDS L2 Ice Thickness, Version 1. http://nsidc.org/data/IRMCR2/versions/1.

Padman L, Siegfried MR and Fricker HA (2018) Ocean Tide Influences on the Antarctic and Greenland Ice Sheets. *Reviews of Geophysics*, 2016RG000546. doi:10.1002/2016RG000546.

Padman L, Fricker HA, Coleman R, Howard S and Erofeeva L (2002) A new tide model for the Antarctic ice shelves and seas. *Annals of Glaciology* **34**, 247–254. doi:10.3189/172756402781817752.

Rignot E, Mouginot J and Scheuchl B (2017) MEaSUREs InSAR-Based Antarctica Ice Velocity Map, Version 2. doi:10.5067/D7GK8F5J8M8R.

Rignot E, Jacobs S, Mouginot J and Scheuchl B (2013) Ice-Shelf Melting Around Antarctica. *Science* **341**(6143), 266–270. doi:10.1126/science.1235798.

Rignot E, Mouginot J and Scheuchl B (2011a) Ice Flow of the Antarctic Ice Sheet. *Science* **333**(6048), 1427–1430. doi:10.1126/science.1208336.

Rignot E, Mouginot J and Scheuchl B (2011b) Antarctic grounding line mapping from differential satellite radar interferometry. *Geophysical Research Letters* **38**(10). doi:10.1029/2011GL047109.

Rignot E and Jacobs SS (2002) Rapid Bottom Melting Widespread near Antarctic Ice Sheet Grounding Lines. *Science* **296**(5575), 2020–2023. doi:10.1126/science.1070942.

Shean DE, Joughin IR, Dutrieux P, Smith BE and Berthier E (2019) Ice shelf basal melt rates from a high-resolution digital elevation model (DEM) record for Pine Island Glacier, Antarctica. *The Cryosphere* **13**(10), 2633–2656. doi:https://doi.org/10.5194/tc-13-2633-2019.

Studinger M (2013) IceBridge ATM L1B Elevation and Return Strength, Version 2. doi:10.5067/19SIM5TXKPGT.

Studinger M (2012) Pre-IceBridge ATM L1B Qfit Elevation and Return Strength, Version 1. doi:10.5067/8Q93SAT2LG3Q.

Summers P and Schroeder D (2022) Evidence for Temperate Ice in Shear Margins of Antarctic Ice Streams from Airborne Radar Surveys. *Twenty-Ninth Annual WAIS Workshop*, 26 September 2022-29 September 2022, YMCA of the Rockies, Estes Park, CO. https://www.waisworkshop.org/2022-wais-workshop.

Vaňková I, Nicholls KW and Corr HFJ (2021) The Nature of Ice Intermittently Accreted at the Base of Ronne Ice Shelf, Antarctica, Assessed Using Phase-Sensitive Radar. *Journal of Geophysical Research: Oceans* **126**(10), e2021JC017290. doi:10.1029/2021JC017290.

Vaňková I and Nicholls KW (2022) Ocean Variability Beneath the Filchner-Ronne Ice Shelf Inferred From Basal Melt Rate Time Series. *Journal of Geophysical Research: Oceans* **127**(10), e2022JC018879. doi:10.1029/2022JC018879.